Energy Storage Materials 14 (2018) 258–266

Contents lists available at ScienceDirect

Energy Storage Materials

journal homepage: www.elsevier.com/locate/ensm

Nanoporous and lyophilic battery separator from regenerated eggshell membrane with effective suppression of dendritic lithium growth

Lianbo Ma[a,1], Renpeng Chen[a,1], Yi Hu[a], Wenjun Zhang[a], Guoyin Zhu[a], Peiyang Zhao[a], Tao Chen[a], Caixing Wang[a], Wen Yan[a], Yanrong Wang[a], Lei Wang[a], Zuoxiu Tie[a], Jie Liu[a,b,*], Zhong Jin[a,**]

[a] Key Laboratory of Mesoscopic Chemistry of MOE, School of Chemistry and Chemical Engineering, Nanjing University, Nanjing 210093, China
[b] Department of Chemistry, Duke University, Durham, NC 27708, USA

ARTICLE INFO

Keywords:
Lithium metal-based batteries
Dendritic lithium
Nanoporous separator
Regenerated eggshell membrane
High-temperature endurance

ABSTRACT

Lithium metal-based batteries are attractive energy storage systems owing to the high theoretical capacity of lithium metal anode and the known lowest potential among existing anodes. However, lithium anodes usually suffer from severe growth of lithium dendrites, a main reason of safety concern. Engineering the structure of separators could be an effective solution for resolving this issue. Herein, we demonstrate that eggshell membrane (ESM) extracted from waste eggshell is a promising candidate as high-performance separator. Furthermore, we have developed a biomimetic and economic strategy to produce large-area and flat regenerated ESM (RESM) to overcome the size and shape limits of raw ESM. The ESM and RESM are highly lyophilic to electrolytes; their well-distributed pores and high electrolyte uptake allow fast ion-diffusion; and their high mechanical and thermal stability ensure the safety and cyclability of batteries. Most impressively, the nanoporous structure and the negatively-charged surface of ESM and RESM separators can effectively suppress the formation of lithium dendrites, even after long-term cycling under high rate. Lithium-ion batteries, lithium-sulfur batteries, and sodium-ion batteries using RESM separators all show boosted rate capability and cycling retention, outperforming commercial separators on almost all fronts. Even at a high temperature (120 °C), lithium-ion batteries with RESM separators can still operate normally. Our findings indicate the nanoporous RESM film can meet most if not all requirements of an ideal separator for metal ion batteries.

1. Introduction

Since the application of batteries has been vigorously expanded into new fields, such as smart electronics, clean-energy vehicles and grid-scale storage, the search for portable, high capacity and safe electrical energy storage technologies has become one of the paramount motivators for battery material research [1–4]. Lithium metal-based secondary batteries, including lithium–air, lithium–metal oxides and lithium–sulfur batteries (LSBs), are attractive alternatives to conventional lithium-ion batteries (LIBs), owning to the high theoretical capacity of lithium metal anode (3860 mA h g^{-1}) and the lowest redox potential among all existing anodes [5,6]. However, for the practical use of lithium metal anode, the severe dendritic lithium formation on the lithium metal surface should be suppressed [7,8]. During the repeated charge-discharge cycling, the continuous uneven deposition and stripping of lithium induce uncontrollable growth of lithium dendrites, which can penetrate through the polymer separator and form micro-short circuits between the positive and negative electrodes, causing the serious safety issues including fire and even explosions [9–12].

In recent years, although great efforts have been made on the optimization of electrolytes [13–16], the achievements on suppressing dendritic lithium growth are still limited, because normally lithium metal cannot conformally contact the separator in microscale during charge/discharge processes. Separators with well-designed nanostructures hold the key for suppressing the growth of lithium dendrites. Traditionally, this problem was clumsily alleviated by using thicker and more tortuous separators. However, such separators normally lead to increased impedance loss, and still cannot fully suppress the dendritic lithium growth [17]. Currently, the most widely-used commercial

* Corresponding author at: Key Laboratory of Mesoscopic Chemistry of MOE, School of Chemistry and Chemical Engineering, Nanjing University, Nanjing 210093, China.
** Corresponding author.
E-mail addresses: j.liu@duke.edu (J. Liu), zhongjin@nju.edu.cn (Z. Jin).
[1] These authors contributed equally.

https://doi.org/10.1016/j.ensm.2018.04.016
Received 13 February 2018; Received in revised form 11 April 2018; Accepted 12 April 2018
Available online 16 April 2018

separators (such as Celgard™-2400 shown in Fig. S1) are made of polyolefin films [18–20], predominantly polyethylene (PE) or polypropylene (PP). Unfortunately, owning to the unsuitable morphology and pore size distribution of commercial separators, the capability for suppressing the formation and growth of lithium dendrites is very limited. Moreover, polyolefin films usually suffer from insufficient electrolyte wettability, low porosity and serious thermal shrinkage [21–25], which are partially responsible for the relatively poor electrochemical performance and poor safety of lithium metal-based batteries. Previous reports have explored the modification of commercial Celgard separator by coating with ceramic or polymer for improving the electrolyte affinity and resistance to thermal shrinkage [26–28]. It is ideal to design and fabricate novel separators that can solve all of the above issues.

Based on the systematic evaluation in lithium metal-based batteries, here we report that the pristine eggshell membrane (ESM) extracted from waste eggshell is a promising candidate of separator with remarkable properties. Moreover, to overcome the curved shape and limited size of raw ESM, we further develop a biomimetic and economic strategy to fabricate large-area and flat nanoporous regenerated ESM (RESM) film from pristine ESM. Interestingly, the nanoporous RESM film can well inherit and even significantly enhance the merits of raw ESM as battery separator. It should be noted that although ESM film was investigated for using in energy related applications, such as supercapacitor, synthesis template or starting material [29–37], but the detailed intrinsic properties, regeneration strategy and effects of ESM film for metal lithium-based secondary batteries still have not been investigated. With the good electrolyte wettability, high electrolyte uptake, good mechanical strength, high thermal stability and well-distributed porous structure of RESM film, the batteries with RESM film can exhibit greatly enhanced performances than those with commercial Celgard separator in terms of battery safety, reversible capacity, rate capability and long-term cycling stability under high rates. Impressively, the three-dimensional nanoporous and flexible RESM film can effectively suppress the dendritic lithium growth during charge/discharge processes and maintain a uniform ionic flux on the lithium metal surface.

2. Experimental section

2.1. Chemicals

The waste eggshells were collected from the canteen of Nanjing University. All other chemicals were purchased from Sinopharm Chemical Reagent Co., Ltd, and were of analytical grade and used without further purification.

2.2. Extraction of egg-shell membranes (ESM)

The waste eggshells were firstly cleaned with deionized water and then immersed into HCl solution (1.0 M) for 6 h to remove the hard $CaCO_3$ outer shells. Then, the resultant ESM were washed with deionized water and dried at room temperature for 12 h.

2.3. Dissolution of ESM

The obtained ESM were cut into small pieces and then added into an alkaline solution containing LiOH/NaOH/urea/H_2O with the weight ratio of 5:7:8:80 under stirring for 10 min. Subsequently, the above solution was stored under refrigeration (− 30 °C) until completely frozen. Then, the frozen solid was thawed and stirred vigorously at room temperature for about 6 h to achieve a transparent solution. After that, the upper air bubbles were removed by centrifugation at 6000 rpm for 5 min, and then the resultant solution was stored at 5 °C.

2.4. Preparation of regenerated egg-shell membranes (RESM)

The resultant ESM solution was dropped into a culture dish (made of polytetrafluoroethylene, PTFE) with the liquid height of about 1.0 mm, and then the culture dish was placed in a water bath at 60 °C for about 24 h. After thoroughly washing with deionized water for several times, the culture dish was kept in the water bath (60 °C) again for another 12 h. Finally, the as-grown RESM were peeled off by tweezers, and dried in a vacuum oven at 40 °C for 24 h.

2.5. Characterizations

Field-emission scanning electron microscopy (SEM) images were collected on a JEOL JSM-6480 scanning electron microscope. Nitrogen adsorption-desorption isotherms were obtained through Brunauer–Emmett–Teller (BET) analysis at 77 K on a Quantachrome Autosorb-IQ-2C-TCD-VP instrument. The elemental compositions of the samples were characterized by an element analyzer (CHN-O-Rapid). The FT-IR spectrum was measured by Fourier transform infrared spectrometer (Nicolet Nexus 470). The contact angles were observed with a dynamic contact angle measuring device/tensiometer (OCA 30, DataPhysics Instruments GmbH). Energy dispersive X-ray spectroscopy (EDX) profiles were taken on a JEOL JEM-2100F transmission electron microscope using an accelerating voltage of 200 kV. Powder X-ray diffraction (XRD) patterns were recorded with an X-ray diffractometer (Bruker D-8 Advance) using Cu Kα (λ = 1.5406 Å) radiation at a scanning rate of 6° min^{-1}. Raman analysis was performed on a Horiba JY Raman spectrometer using a 473 nm laser source. Thermogravimetric analysis (TGA) was performed on a NETZSCH STA-449-C instrument under N_2 atmosphere at a heating rate of 10 °C min^{-1}.

2.6. Calculation methods

The stress versus strain profiles of the separator films were measured using an Instron-3300 universal tensile tester at a speed of 10 mm min^{-1} using the samples with 1.0 cm in width and 8.0 cm in length. The Young's modulus was calculated by Eq. (1):

$$E = \sigma/\varepsilon \quad (1)$$

where σ and ε represent the stress and strain of the separator, respectively.

The electrolyte uptakes of separators were measured by immersing into the designated battery electrolyte, and calculated according to Eq. (2):

$$E_{uptake} = (Wd - Wt)/Wt \quad (2)$$

where *Wt* represents the weight of the separator, and *Wd* is the weight of the separator after filled with electrolyte.

The porosity of the separators was calculated based on Eq. (3):

$$\text{Porosity } (\%) = [1 - (W/\rho)]/(A \times t) \quad (3)$$

where W is the weight of the separator, ρ is the density of the separator, *A* is the area of the separator, and *t* is the thickness of the separator.

2.7. Preparation of carbon nanotube-sulfur (CNTs-S) composite as cathode material for lithium-sulfur batteries (LSBs)

Briefly, 40 mg of CNTs (TimeNano, China) was mixed with 60 mg of pure sulfur powder in an agate mortar. The mixture was transferred into an autoclave and heated at 155 °C for 12 h. Then, the product was further heated in a tube furnace at 200 °C for 30 min under Ar atmosphere to remove the excess sulfur.

2.8. Preparation of hierarchical porous nitrogen-rich carbon (HPNC) nanospheres as anode material for sodium-ion batteries (SIBs)

Typically, 264 mg of zinc acetate dihydrate ($Zn(Ac)_2{\cdot}2H_2O$) and 800 mg of polyvinyl pyrrolidone (PVP) were dissolved into 40 mL of deionized water under stirring. Subsequently, 20 mL of tripotassium hexacyanocobaltate ($K_3[Co(CN)_6]$) (266 mg) aqueous solution was added into the above mixture solution under ultrasonication at 0 °C. After stirring for 1 h, the mixture was aged for 6 h. Then, the precipitate was collected by centrifugation, washed with deionized water, and dried in a vacuum oven at 60 °C for 12 h. The powder was annealed at 700 °C for 2 h in N_2 atmosphere with a heating rate of 2 °C min^{-1}, followed by etching successively in hydrofluoric acid (HF, 5 wt%) and hydrochloric acid (HCl, 1.0 M) solution. Finally, the product was washed with deionized water and absolute ethanol for several times, and dried at 60 °C in a vacuum oven.

2.9. Electrochemical tests of batteries

The working electrodes were prepared by mixing the active materials, acetylene black and binder (polyvinylidene fluoride, PVDF) with a weight ratio of 80:10:10 in N-methyl-pyrrolidinone (NMP), and then stirred for 24 h to form a homogeneous electrode ink.

The $LiFePO_4$/Li coin cells were assembled as a model of lithium metal-based batteries. The active material was commercial $LiFePO_4$ powder. The $LiFePO_4$ electrode ink was spread on a copper foil and dried in a vacuum oven at 60 °C to remove the solvent. The coin cells (CR2032) were assembled in an Ar-filled glove box with the $LiFePO_4$ working electrode and lithium foil as the counter electrode. The electrolyte of LIBs used in this study was 1.0 M $LiPF_6$ in the mixture of ethylene carbonate and diethyl carbonate (1:1 in volume) as the electrolyte. The loading mass of $LiFePO_4$ was about 1.6–1.8 mg cm^{-2}.

For the assemble of LSBs, the CNTs-S electrode ink was spread and vacuum-dried on an aluminum foil to serve as the cathode. Lithium foil was employed as the anode. The electrolyte of LSBs used in this study was 1.0 M lithium bis(trifluoromethane) sulfonimide and 0.1 M $LiNO_3$ in the mixture of 1,3 dioxolane and 1,2-dimethoxyethane (1:1 in volume). The loading mass of sulfur was about 1.4–1.6 mg cm^{-2}.

For the assemble of SIBs, the HPNC electrode ink was casted and vacuum-dried on a copper foil to serve as the anode. Sodium metal foil was used as the cathode. The electrolyte of SIBs used in this study is 1.0 M $NaClO_4$ solution in propylene carbonate (PC). The loading mass of HPNC material was about 1.2–1.4 mg cm^{-2}.

For comparisons, Celgard film (Celgard™-2400), ESM and RESM were individually tested as the separators of the above batteries. The electrochemical properties of batteries were measured on a LAND battery test system (Wuhan LAND Electronics Co., Ltd.). The specific capacities of batteries were calculated based on the total weight of active materials.

3. Results and discussion

Fig. 1**a** shows the typical structure of bird or reptile eggs, which usually possess three protective layers: the hard eggshell, the outer ESM and the inner ESM. The hard eggshell is mainly composed of $CaCO_3$ crystals stabilized by protein matrix, while the outer and inner ESM are primarily composed of a porous matrix of interwoven protein fibers and polysaccharides (glycans) [38,39]. After the evolution by the Mother Nature for billions of years, ESM has developed numerous functions and merits including good protection ability of the fertilized eggs from harsh external environment, great permeability for both air and water, considerable cold/heat resistance and biocompatibility. Fig. 1**b** presents the schematic illustration of the synthesis of RESM film. Pristine ESM was extracted from waste eggshell through the etching of $CaCO_3$. Then the compositions of ESM were treated in NaOH/urea/LiOH solution and completely dissolved, owing to the swelling and solation of hydrophilic biomatters (proteins and glycans, *etc.*) through the break of hydrogen bonds in the mixed alkali solution. Finally, the dissolved compositions were re-assembled to RESM at 60 °C in a culture dish as the deposition substrate, forming a uniform

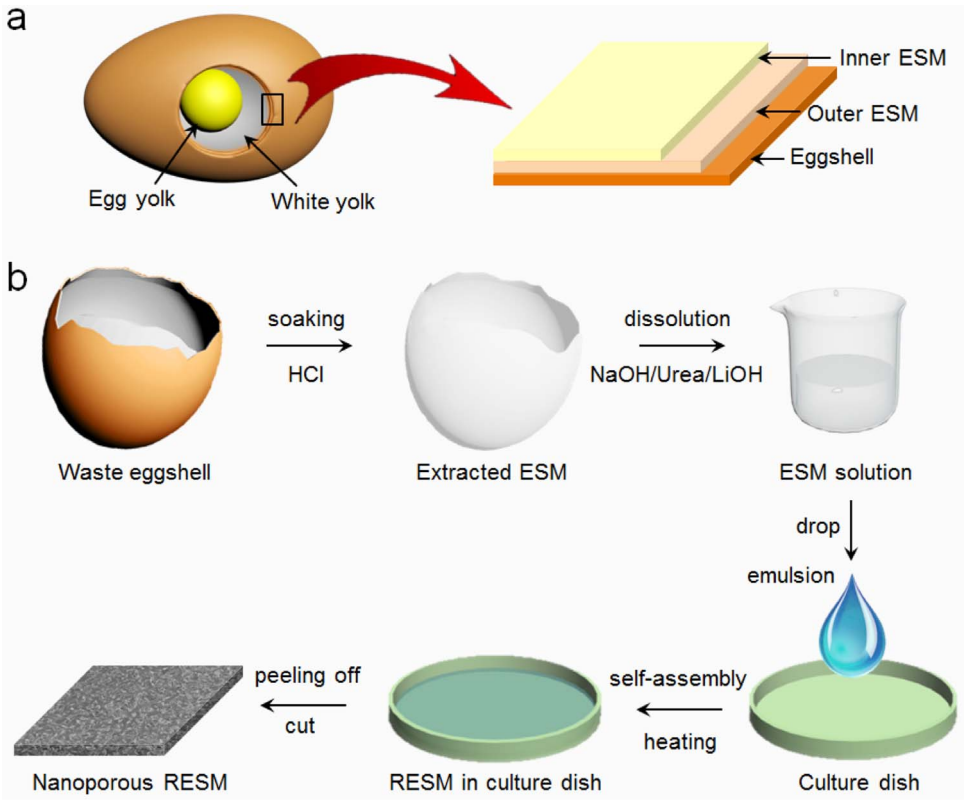

Fig. 1. (a) Structural diagrams of egg and eggshell. (b) Schematical illustration of the preparation process of RESM.

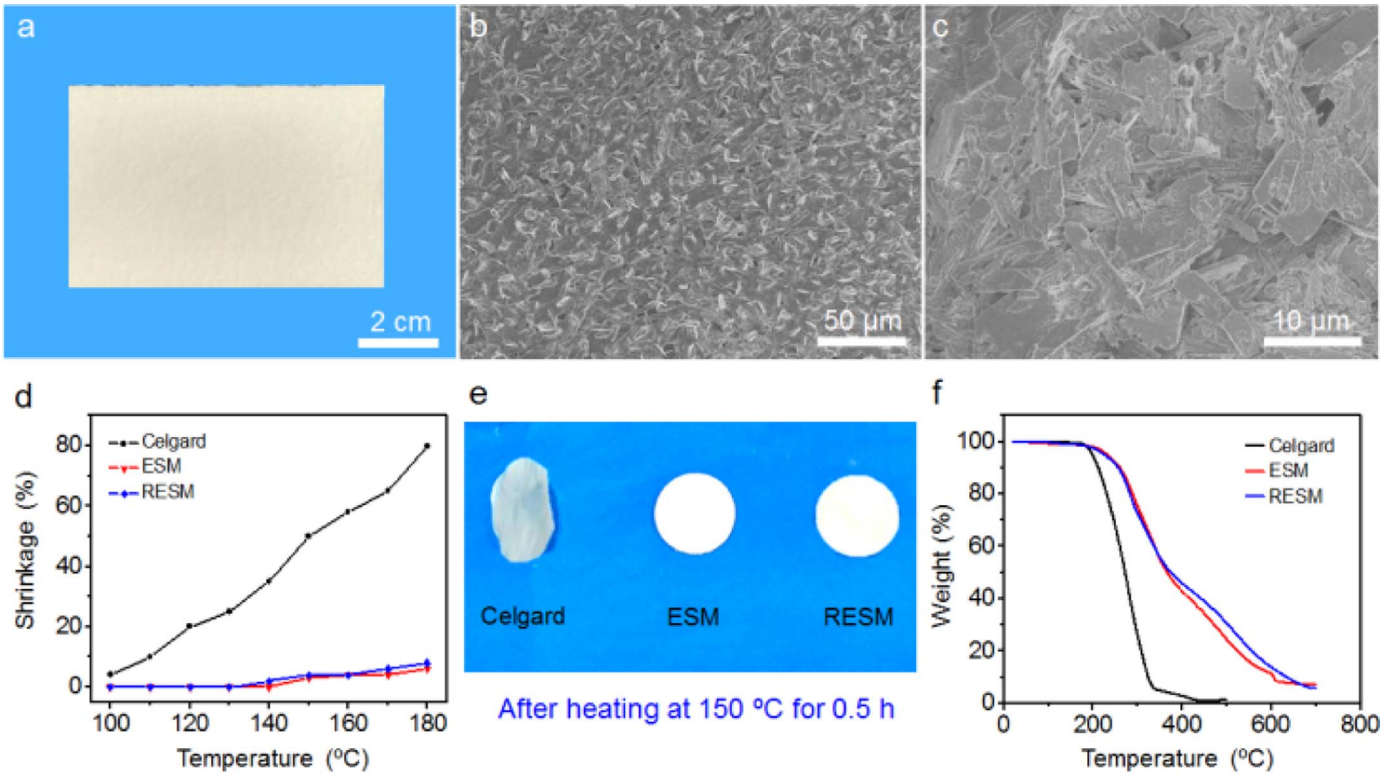

Fig. 2. (a) Optical photograph of large-area RESM after cutting to a rectangular shape. (b, c) SEM images of RESM at different magnifications. (d) Dimensional shrinkage of Celgard film, ESM and RESM at different temperatures. (e) Photographs of Celgard film, ESM and RESM after heating at 150 °C for 0.5 h. (f) TGA curves of Celgard film, ESM and RESM under N_2 atmosphere.

two-dimensional membrane with nanoporous structures. Notably, the RESM well-retained the intrinsic advantages of raw ESM, such as the lyophilic nature, well-distributed pores and high thermal stability. Unlike common polymer-based separators, the production of RESM separators is a facile, economic, environment-friendly and sustainable process that can turn waste into treasure.

The pristine ESM (Fig. S2) exhibits a naturally-formed "nonwoven fabric" structure with curved shape, porous surface and an average thickness of ~ 50 μm, mainly consisting of interconnected microfibers with the diameter between 3 and 16 μm. The microfibers in ESM are mostly composed of interwoven protein fibers and glycan chains [40], which contribute to the good electrolyte wettability and can effectively avoid the dendritic lithium growth and internal short-circuit during the charge/discharge cycles (as detailed below). As shown in Fig. S2 and Fig. S3, the interconnected microfibers formed abundant pores with the sizes varied in the range of ~ 12 nm to several microns [41,42].

The RESM well preserved the original flexible structure of raw ESM. Fig. 2**a** presents a photograph of RESM after cutting to a rectangular shape, showing the large-area flat surface different from the size-limited and curved surface of raw ESM. The morphology of RESM was characterized by scanning electron microscopy (SEM, Fig. 2**b, c**), indicating a porous microstructure consisting of bio-microfibers and microrods re-assembled from original ESM. Notably, the thickness of RESM can be finely tuned from several to hundreds of micrometers by varying the solution concentration of dissolved ESM.

The surface areas and pore size distributions of both ESM and RESM were examined by the N_2 adsorption-desorption isotherms. As indicated in Fig. S3, the measured specific surface areas of ESM and RESM were 18.4 and 23.2 m^2 g^{-1}, and the pore volume are 0.24 and 0.31 cm^3 g^{-1}, respectively. Moreover, the ESM and RESM show the similar pore size distributions (13.5 nm for ESM and 15.6 nm for RESM, respectively), and much smaller than that of commercial Celgard™-2400 (117 nm × 42 nm, technical data from the Celgard LLC, USA). The compositions of RESM examined by elemental analysis include C, N and H elements (31.9, 11.6 and 5.5 wt%, respectively), comparable with those of pristine ESM (34.8, 10.7 and 6.1 wt.%, respectively). Further Fourier transform infrared spectroscopy (FT-IR) spectra of ESM and RESM films in Fig. S4 show the characteristic peaks corresponding to -NH/-NH_2 groups (3448 cm^{-1}), -CH_2 groups (2932 cm^{-1}), imine groups (1647 cm^{-1}), and triazine groups (1535 cm^{-1}). These results confirm that ESM and RESM films possess a large number of nitrogen-containing functional groups with high polarity and lyophilicity, leading to strong affinity with Li^+ and efficient suppression of Li dendrite growth during electrochemical processes [12]. The measured Young's modulus of both ESM and RESM are comparable (~ 560 MPa), which is much higher than that of commercial Celgard-2400 film (~ 300 MPa), implying the ESM and RESM can better retain the structural integrity and avoid the rupture under physical disruption.

Small thermal shrinkage is essential for separators to achieve good high-temperature stability [43–46]. The dimensional shrinkage of Celgard film, ESM and RESM were measured at different temperatures (Fig. 2**d**). Both ESM and RESM exhibited very small shrinkage as the temperature increased to 180 °C, while the Celgard film showed an obvious shrinkage at temperatures above 150 °C. Fig. 2**e** presents the photographs of Celgard film, ESM and RESM after heating at 150 °C for 0.5 h, demonstrating the much better structural retention of ESM and RESM than that of Celgard film. Thermogravimetric analysis (TGA, Fig. 2**f**) shows the ESM and RESM begin to lose weight at ~ 260 °C, owing to the degradation of collagen and glycan chains. In contrast, the Celgard film begins to decompose at ~ 180 °C, and has a large weight loss of ~ 75% at 300 °C. These results indicate that the ESM and RESM films have much higher thermal stability than commercial Celgard separator.

Wettability and electrolyte uptake are important parameters for separators [47–49]. The contact angles of deionized water and secondary battery electrolytes (including the electrolytes of LIBs, LSBs and sodium-ion batteries (SIBs), the chemical compositions are

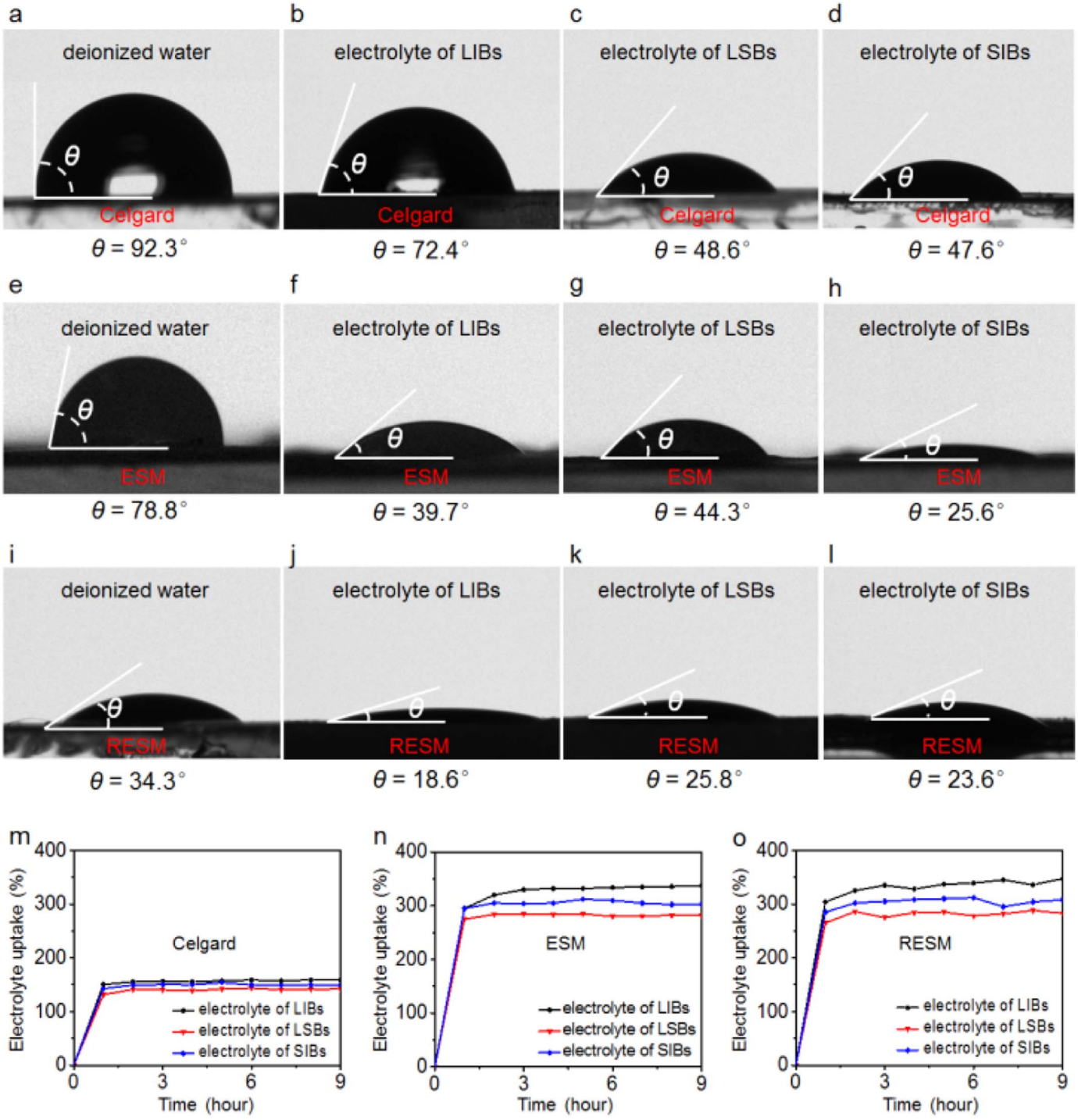

Fig. 3. (a-l) Contact angle images of Celgard film (a-d), ESM (e-h) and RESM (I-L) with (a, e, i) deionized water, (b, f, j) electrolyte of LIBs, (c, g, k) electrolyte of LSBs and (d, h, l) electrolyte of SIBs, respectively. (m-o) The electrolyte uptakes of (m) Celgard film, (n) ESM and (o) RESM with different electrolytes.

detailed in the Experimental section of Supporting information) on the surface of Celgard film, ESM and RESM were investigated, respectively, as shown in Fig. 3. Compared to Celgard film, both ESM and RESM show remarkably reduced contact angles for all tested liquids, suggesting the much better lyophilic properties. Interestingly, the hydrophilicity of RESM (θ = 34.3°) is even higher than pristine ESM (θ = 78.8°), probably due to the treatment in alkaline solutions and the variation of surface texture after regeneration. Moreover, Fig. S5 shows that both ESM and RESM can adsorb the above electrolytes much better than Celgard film, and further verify that RESM are more lyophilic. The higher electrolyte wettability of ESM and RESM can be attributed to the highly lyophilic nature of collagen and glycan compositions. The electrolyte uptake capacities of these films were also compared quantitatively, as shown in Fig. 3**m-o**. The weight ratios of electrolyte uptake increase rapidly at the initial stages and then slowly reach the maximum levels. For the electrolytes of LIBs, LSBs and SIBs, the maximum uptake capacities of ESM (320%, 280% and 300%, respectively) and RESM (340%, 270% and 290%, respectively) are about two times higher than those of Celgard film (135%, 150% and 155%, respectively). Moreover, the porosity of ESM (43%, calculated with Eq. S3) and RESM (48%) are higher than that of Celgard film (37%), suggesting the better performance to hold sufficient electrolyte between

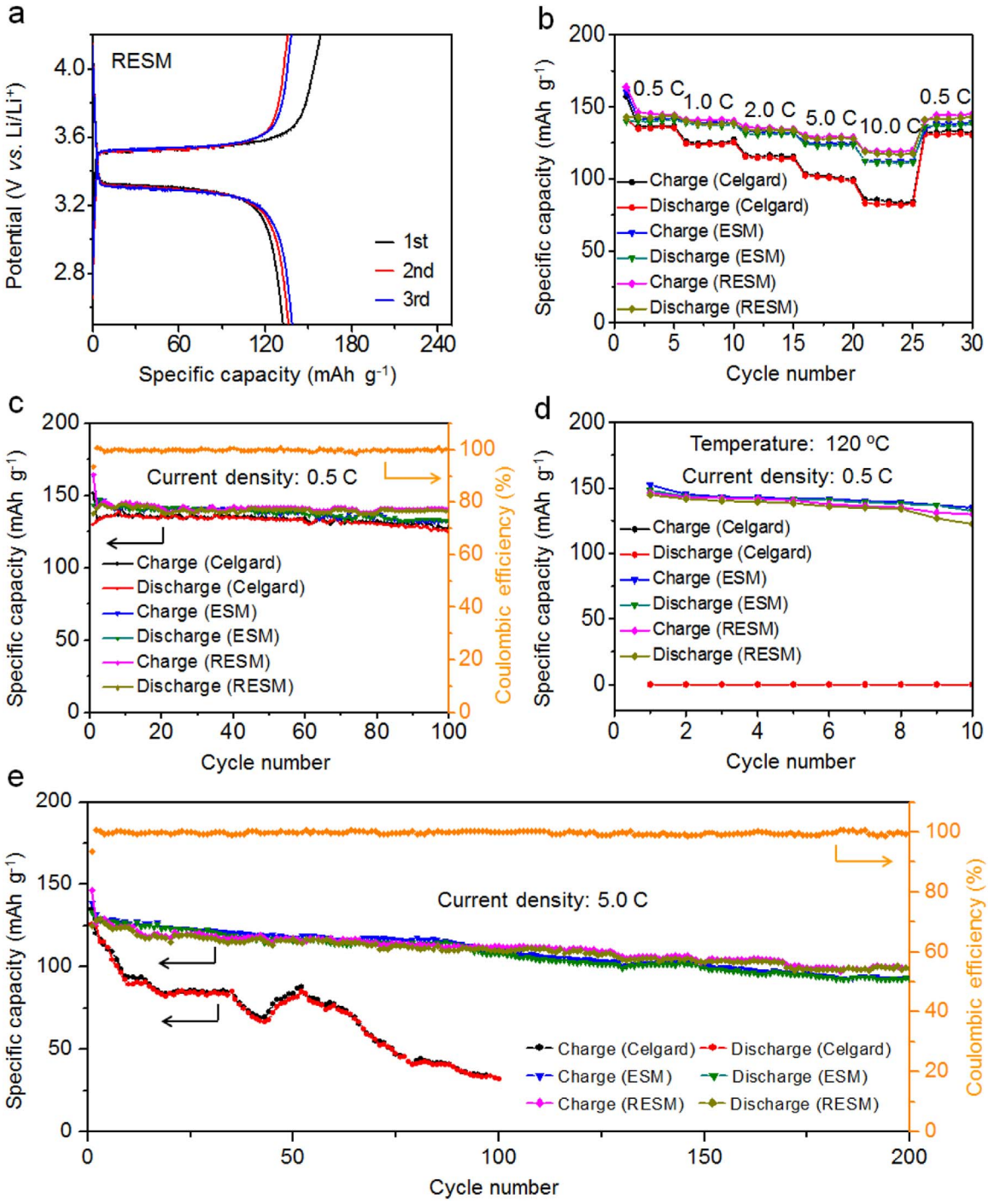

Fig. 4. (a) Galvanostatic charge/discharge profiles of $LiFePO_4$/Li cells with RESM separators at 0.5 C within the potential range of 2.5–4.2 V vs. Li/Li^+. (b) Rate capability of $LiFePO_4$/Li cells with different separators. (c) Cycling performance of $LiFePO_4$/Li cells at 0.5 C under the default temperature of 25 °C and the corresponding Coulombic efficiency of $LiFePO_4$/Li cells with RESM. (d) Cycling performance of $LiFePO_4$/Li cells at 0.5 C under an elevated temperature of 120 °C. (e) Long-term cycling stability comparison of $LiFePO_4$/Li cells with different separators at 5.0 C and the corresponding Coulombic efficiency of $LiFePO_4$/Li cells with RESM.

electrodes [50]. The highly porous and lyophilic microstructure of ESM and RESM are the main reasons of greatly improved electrolyte uptake capacities.

The outstanding properties of ESM and RESM are further demonstrated in secondary battery tests, as exhibited in Fig. 4 and Figs. S6–S14. The assessments of $LiFePO_4$/Li cells with different separators (Celgard separator, ESM and RESM) and all other identical conditions are presented in Fig. 4. The first three galvanostatic charge/discharge profiles of $LiFePO_4$/Li cells with these separators at 0.5 C show similar plateaus and almost overlapped curves at the 2nd and 3rd cycles (Fig. 4**a** and Fig. S6). However, the $LiFePO_4$/Li cells with ESM or RESM separators exhibit much higher rate capability than those with Celgard film separators, as shown in Fig. 4**b**. At a high rate of 10.0 C, the discharge capacities of $LiFePO_4$/Li cells with ESM and RESM separators are 111 and 117 mA h g^{-1}, respectively, meanwhile those with Celgard film separators only deliver a discharge capacity of only 83 mA h g^{-1}. The superior rate capabilities should be ascribed to the high ionic conductivity and low interfacial resistance of ESM and RESM [51,52], as evidenced by the Nyquist plots in Fig. S7, which confirms that the $LiFePO_4$/Li cells with ESM or RESM separators have

lower contact resistance and lower charge-transfer resistance than those with Celgard film separators.

The cycling stability and high-temperature safety of these separators were examined. At a normal working temperature of 25 °C (Fig. 4**c**), the $LiFePO_4$/Li cells with Celgard film, ESM and RESM as separators show comparable initial discharge capacities (130, 143 and 138 mA h g^{-1} at 0.5 C, respectively) and good cycling stability (125, 133 and 140 mA h g^{-1} after 100 consecutive cycles at 0.5 C, respectively). However, the high-temperature tolerance of ESM and RESM are far superior to Celgard film. As revealed in Fig. 4**d**, the $LiFePO_4$/Li cells with ESM or RESM separators can sustain stable charge/discharge curves at even 120 °C. In contrast, those with Celgard film separators cannot be charged/discharged properly, which should be ascribed to the short circuit induced by the high-temperature shrinkage of Celgard film (as noted above).

The long-term cycling performance of at high rates were also investigated (Fig. 4**e**). The $LiFePO_4$/Li cells with ESM and RESM separators show significantly improved cycling stability compared to those with Celgard film separators. At a high rate of 5.0 C, the $LiFePO_4$/Li cells with ESM and RESM separators present high initial discharge capacities (133 and 126 mA h g^{-1}, respectively) and good stability (108 and 112 mA h g^{-1} after 100 cycles, 92 and 100 mA h g^{-1} after 200 cycles, respectively). In contrast, the discharge capacity of those with Celgard film separators is only 32 mA h g^{-1} after 100 cycles.

To examine the severity of dendritic lithium growth, the surfaces of lithium metal electrodes after long-term cycling under 5.0 C in $LiFePO_4$/Li cells with Celgard, ESM and RESM separators were characterized (Fig. 5). As shown in Fig. 5**a**, the lithium electrode cycled with commercial Celgard separator exhibit the extensive formation of rod-like lithium dendrites, which would continuously expose fresh Li metal surfaces to the electrolyte, and thus, additional solid electrolyte interphase (SEI) layers are generated and the electrolyte solution are gradually consumed [6]. Moreover, lithium dendrites can become isolated from the lithium electrode after long-term cycling with Celgard separator, and the isolated lithium can then react with the organic electrolyte, thus severely degrading the cycling performance. The lithium electrode cycled with ESM separator (Fig. 5**b**) shows much less dendritic morphology than that with commercial Celgard. Remarkably, the lithium deposition in $LiFePO_4$/Li cell with RESM separator (Fig. 5**c**) are even more uniform and flat compared to that with ESM separator. Furthermore, the surface morphology evolution of commercial Celgard, ESM and RESM films after electrochemical tests was also examined. As show in Fig. S15, the commercial Celgard separator after long-term cycling exhibited very rough surface characteristics with severely formed bulges, while ESM and RESM separators after electrochemical tests present much smoother surface characteristics. Therefore, it can be concluded that both ESM and RESM can effectively suppress the dendritic lithium growth by facilitating the uniform distribution of Li^+ over the entire lithium surface (Fig. 5**d-f**). The effective suppression of dendritic lithium formation and growth was also confirmed by the Li/Li symmetric cell tests. Fig. S16 compares the voltage profiles of the Li/Li symmetric cells cycling at 0.5 mA cm^{-2} with an areal capacity of 1.0 mA h cm^{-2}. It was observed that the Li/Li symmetric cells with ESM and RESM separators exhibited much more

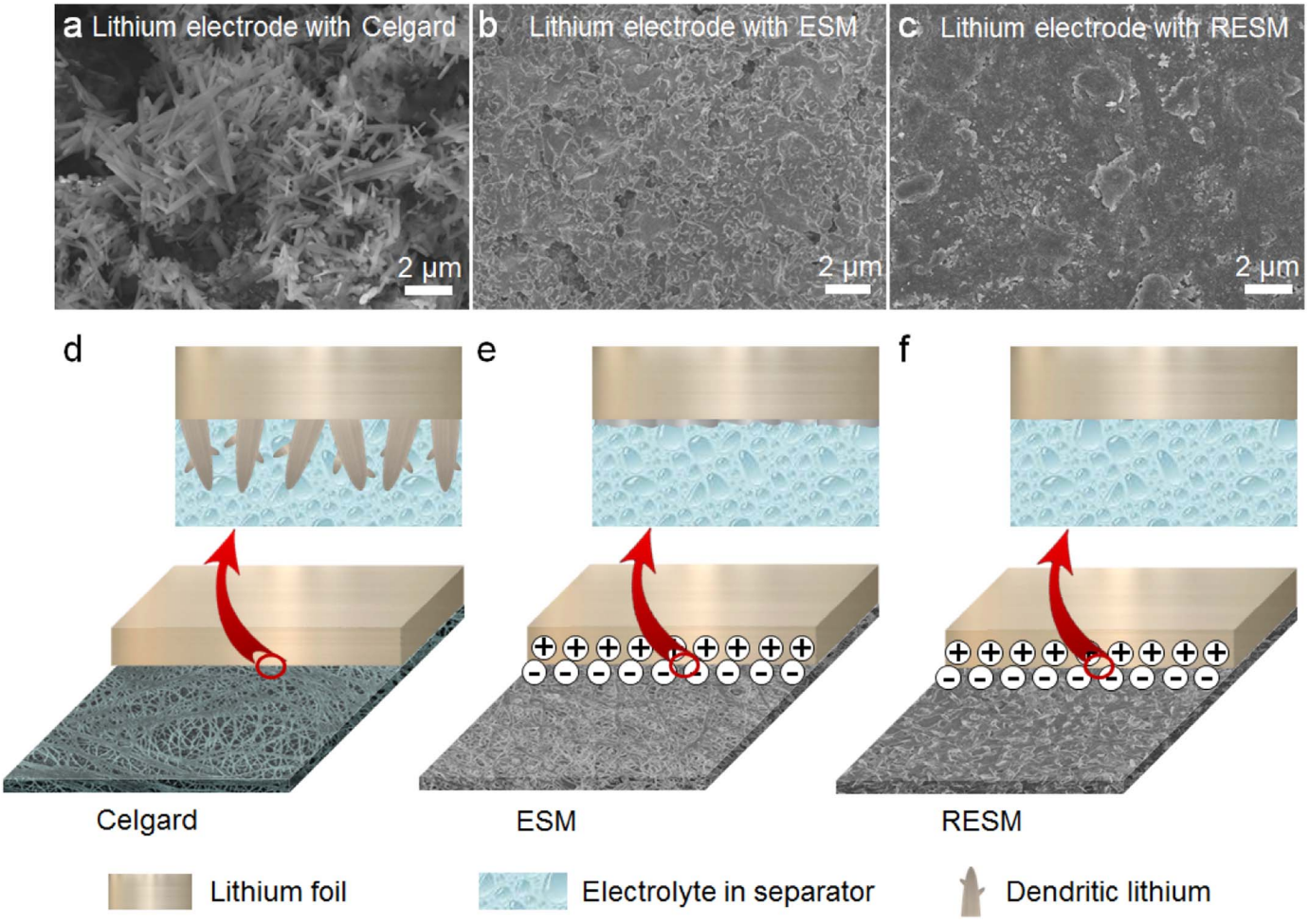

Fig. 5. (a-c) SEM images of lithium metal electrodes after long-term cycling under 5.0 C in $LiFePO_4$/Li cells with (a) commercial Celgard, (b) ESM, and (c) RESM separators, respectively. (d-f) Schematic illustrations of dendritic lithium growth on the lithium metal electrodes in the presence of (d) commercial Celgard, (e) ESM, and (f) RESM separators, respectively.

stable voltage profiles and lower overpotentials than those with commercial Celgard separator. The Li/Li symmetric cell with commercial Celgard separator displayed large voltage hysteresis, which could be attributed to the increased impedance caused by the dendritic lithium formation and growth [53,54]. The suppression of dendritic lithium growth of ESM and RESM is mainly attributed to the nanoporous structure of ESM/RESM and the enhanced interfacial interactions between ESM/RESM and lithium metal electrodes. Unlike commercial Celgard separator, the ESM and RESM have intrinsically lyophilic compositions, thus can form a negative charge layer throughout the surfaces. The electrostatic attraction between the negative charge layers on ESM/RESM and the surface of positively charged lithium metal strongly enhances the interfacial affinity and interaction. Furthermore, superior to the micro-scale pores of Celgard separator, the nano-scale porosity of ESM and RESM can greatly suppress the growth of large-sized lithium dendrites. Therefore, the effective suppression of lithium dendrite growth with ESM and RESM separators can greatly enhance the cycling performance of $LiFePO_4$/Li cells. Additionally, the nanoporous structure of ESM and RESM can enable better electrolyte retention, which may also play a key role on the improvement of battery performance [55,56].

The advantages of ESM and RESM as promising separators for LSBs and SIBs were also confirmed experimentally, as detailed in Supporting Information and Figs. S8–14. The performances of ESM and RESM separators in LSBs and SIBs are both remarkable and far superior to Celgard film, demonstrating the enormous potential for applications in next-generation secondary batteries. The enhanced electrochemical performances can be mainly attributed to the structural superiorities of ESM and RESM films, including higher mechanical and thermal stability, better wettability, higher electrolyte uptake and compact interfacial interactions between ESM/RESM separators and lithium metals, as compared with those of commercial Celgard separator.

4. Conclusions

In summary, we show that the ESM and RESM acquired from abundant and renewable poultry sources can be used as close-to-ideal battery separators that fully outperforming the existing mainstream option. A key finding is the suppression of dendritic lithium growth when using lithium metal electrodes, solving a long standing problem in lithium metal based batteries. Finally, an effective method with high compatibility to current technologies was developed to prepare large-area and flat RESM from size-limited and curved ESM, making it a reality to convert a bio-waste into a crucial component in energy storage devices. Such membranes are very promise to improve the safety and capabilities of various batteries.

Acknowledgements

This work is supported by National Key R & D Program of China (2017YFA0208200, 2016YFB0700600 and 2015CB659300), Projects of NSFC (21403105 and 21573108), Natural Science Foundation of Jiangsu Province (BK20150583 and BK20160647) and the Fundamental Research Funds for the Central Universities (020514380107).

Appendix A. Supporting information

Supplementary data associated with this article can be found in the online version at doi:10.1016/j.ensm.2018.04.016.

References

[1] J.B. Goodenough, K.S. Park, The Li–ion rechargeable battery: a perspective, J. Am. Chem. Soc. 135 (2013) 1167–1176.
[2] C.K. Chen, H.L. Peng, G. Liu, K. Mcllwrath, X.F. Zhang, R.A. Huggins, Y. Cui, High–performance lithium battery anodes using silicon nanowires, Nat. Nanotechnol. 3 (2008) 31–35.
[3] S.S. Zhang, A review on the separators of liquid electrolyte Li–ion batteries, Science 334 (2011) 928–935.
[4] D. Bruce, K. Haresh, J.M. Tarascon, Electrical energy storage for the grid: a battery of choices, Nature 414 (2001) 332–337.
[5] J.M. Tarascon, M. Armand, Issues and challenges facing rechargeable lithium batteries, Nature 414 (2001) 359–367.
[6] D. Aurbach, E. Zinigrad, Y. Cohen, H. Teller, A short review of failure mechanisms of lithium metal and lithiated graphite anodes in liquid electrolyte solutions, Solid State Ion. 148 (2002) 405–416.
[7] K. Liu, A. Pei, H.R. Lee, B. Kong, N. Liu, D.C. Lin, Y.Y. Liu, C. Liu, P. Hsu, Z.N. Bao, Y. Cui, Lithium metal anodes with an adaptive “solid-liquid” interfacial protective layer, J. Am. Chem. Soc. 139 (2017) 4815–4820.
[8] M. Armand, J.M. Tarascon, Building better batteries, Nature 451 (2008) 652–657.
[9] H. Kim, G. Jeong, Y.U. Kim, J.H. Kim, C.M. Park, H.J. Sohn, Metallic anodes for next generation secondary batteries, Chem. Soc. Rev. 42 (2013) 9011–9034.
[10] Z. Li, J. Huang, B. YannLiaw, V. Metzler, J. Zhang, A review of lithium deposition in lithium-ion and lithium metal secondary batteries, J. Power Sources 254 (2014) 168–182.
[11] L. Fan, S.Y. Wei, S.Y. Li, Q. Li, Y.Y. Lu, Recent progress of the solid-state electrolyte for high-energy metal-based batteries, Adv. Energy Mater. 451 (2018) 1702657.
[12] L. Fan, H.L. Zhuang, W.D. Zhang, Y. Fu, Z.H. Liao, Y.Y. Lu, Stable lithium electrodeposition at ultra-high current densities enabled by 3D PMF/Li composite anode, Adv. Energy Mater. 351 (2018) 1703360.
[13] Y.Y. Lu, Z. Tu, L.A. Archer, Stable lithium electrodeposition in liquid and nanoporous solid electrolyte, Nat. Mater. 13 (2014) 961–969.
[14] Y.Y. Lu, S.K. Das, S.S. Moganty, L.A. Archer, Ionic liquid-nanoparticle hybrid electrolytes and their application in secondary lithium-metal batteries, Adv. Mater. 24 (2012) 4430–4435.
[15] N. Kamaya, K. Homma, Y. Yamakawa, M. Hirayama, R. Kanno, M. Yonemura, T. Kamiyama, Y. Kati, S. Hama, K. Kawamoto, A. Mitsui, A lithium superionic conductor, Nat. Mater. 10 (2011) 682–686.
[16] W. Xu, J.L. Wang, F. Ding, X.L. Chen, E. Nasybulin, Y.H. Zhang, J.G. Zhang, Lithium metal anodes for rechargeable batteries, Energy Environ. Sci. 7 (2014) 513–537.
[17] W.K. Shin, A.G. Kannan, D.W. Kim, Effective suppression of dendritic lithium growth using an ultrathin coating of nitrogen and sulfur codoped graphene nanosheets on polymer separator for lithium metal batteries, ACS Appl. Mater. Interfaces 7 (2015) 23700–23707.
[18] Z.G. Yang, J.L. Zhang, M.C.W. Kintner-Meyer, X.C. Lu, D.W. Choi, J.P. Lemmon, J. Liu, Electrochemical energy storage for green grid, Chem. Rev. 111 (2011) 3577–3613.
[19] Y. Wang, J. Travas-Sejdic, R. Steiner, Polymer gel electrolyte supported with microporous polyolefin membranes for lithium ion polymer battery, Solid State Ion. 148 (2002) 443–449.
[20] X.S. Huang, Separator technologies for lithium–ion batteries, J. Solid State Electrochem. 15 (2011) 649–662.
[21] M.H. Ryou, Y.M. Lee, J.K. Park, J.W. Choi, Mussel-Inspired polydopamine-treated polyethylene separators for high-power Li-ion batteries, Adv. Mater. 23 (2011) 3066–3070.
[22] Y.C. Zhang, Z.H. Wang, H.F. Xiang, P.C. Shi, H.H. Wang, A thin inorganic composite separator for lithium-ion batteries, J. Membr. Sci. 509 (2016) 19–26.
[23] X.L. Dong, W.L. Mi, L.H. Yu, J. Yi, Y.S. Lin, Zeolite coated polypropylene separators with tunable surface properties for lithium-ion batteries, Microporous Mesoporous Mater. 226 (2016) 406–414.
[24] H.S. Jeong, J.H. Kim, S.Y. Lee, A novel poly(vinylidene fluoride-hexafluoropropylene)/Poly(ethylene terephthalate) composite nonwoven separator with Phase Inversion-controlled microporous structure for a lithium-ion battery, J. Mater. Chem. 20 (2010) 9180–9186.
[25] H. Lee, M. Alcotlabi, J.V. Watson, X.W. Zhang, Electrospun nanofiber-coated separator membranes for lithium-ion rechargeable batteries, J. Appl. Polym. Sci. 129 (2013) 1939–1951.
[26] M.H. Ryou, D.J. Lee, J.N. Lee, Y.M. Lee, J.P. Park, J.W. Choi, Excellent cycle life of lithium-metal anodes in lithium-ion batteries with mussel-inspired polydopamine-coated separators, Adv. Energy Mater. 2 (2012) 645–650.
[27] C.H. Zhu, T. Nagaishi, J. Shi, H. Lee, P.Y. Wong, J.H. Sui, K.J. Hyodo, I.S. Kim, Enhanced wettability and thermal stability of a novel polyethylene terephthalate-based poly(vinylidene fluoride) nanofiber hybrid membrane for the separator of lithium-ion batteries, ACS Appl. Mater. Interfaces 9 (2017) 21971–21978.
[28] X. Li, J.H. Tao, D.H. Hu, M.H. Engelhard, W.G. Zhao, J.G. Zhang, W. Xu, Stability of polymeric separators in lithium metal batteries in a low voltage environment, J. Mater. Chem. A 6 (2018) 5006–5015.
[29] H.J. Yu, Q.W. Tang, J.H. Wu, Y.Z. Lin, L.Q. Fan, M.L. Huang, J.M. Lin, Y. Li, F.D. Yu, Using eggshell membrane as a separator in supercapacitor, J. Power Sources 206 (2012) 463–468.

[30] C.Z. Wei, H.F. Ma, F. Gao, Green synthesis of metal/C and metal oxide/C films by using nature membrane as support, Front. Mater. Sci. 8 (2014) 150–156.
[31] J.J. Alcaraz, M. Jarib, P. Celso, H.P. deOliveira, Fabrication of highly flexible hierarchical polypyrrole/carbon nanotube on eggshell membranes for supercapacitors, ACS Omega 2 (2017) 2866–2877.
[32] X.H. Meng, D. Deng, Trash to treasure: waste eggshell as chemical reactors for the synthesis of amorphous $Co(OH)_2$ nanorod arrays on various substrates for applications in rechargeable alkaline batteries and electrocatalysis, ACS Appl. Mater. Interfaces 9 (2017) 5244–5253.
[33] S.H. Chung, C.H. Chang, A. Manthiram, Hierarchical sulfur electrodes as a testing platform for understanding the high-loading capability of Li-S batteries, J. Power Sources 334 (2016) 179–190.
[34] J.F. Li, W. Zhang, G.T. Zan, Q. Wu, A high-performance dual-function material: self-assembled super long alpha-Fe_2O_3 hollow tubes with multiple heteroatom (C-, N- and S-) doping, Dalton Trans. 45 (2016) 12790–12799.
[35] X.H. Meng, D. Deng, Trash to treasure: waste eggshell used as reactor and template for synthesis of Co_9S_8 nanorod arrays on carbon fibers for energy storage, Chem. Mater. 28 (2016) 3897–3904.
[36] X.H. Liu, C.Y. Yin, J. Yang, M.Y. Liang, J.J. Wei, Z.Y. Zhang, H.L. Wang, Q.G. Wang, Controllable preparation of an eggshell membrane supported hydrogel electrolyte with thickness-dependent electrochemical performance, J. Mater. Chem. A 4 (2016) 17933–17938.
[37] Z. Li, L. Zhang, B.S. Amirkhiz, X.H. Tan, Z.W. Xu, H.L. Wang, B.C. Olsen, C.M.B. Holt, D. Mitlin, Carbonized chicken eggshell membrane with 3D architectures as high-performance electrode materials for supercapacitors, Adv. Energy Mater. 2 (2012) 431–437.
[38] Y. Nys, J. Gautron, J.M. Garcia-Ruiz, M.T. Hincke, Avian eggshell mineralization: biochemical and functional characterization of matrix proteins, Comptes Rendus Palevol 3 (2004) 549–562.
[39] I. Lavelin, N. Meiri, M. New, insight in eggshell formation, Poult. Sci. 79 (2000) 1014–1017.
[40] F. Yi, Z.X. Guo, L.X. Zhang, J. Yu, Q. Li, Soluble eggshell membrane protein: preparation, characterization and biocompatibility, Biomaterials 25 (2004) 4591–4599.
[41] D.H. Wang, Y.J. Li, L. Liu, J.S. Liu, M. Bao, N. Yang, Z.C. Hou, Z.H. Ning, Traits of eggshells and shell membranes of translucent eggs, Poult. Sci. 96 (2017) 351–358.
[42] A. Riley, C.J. Sturrock, S.J. Mooney, M.R. Luck, Quantification of eggshell microstructure using X-ray micro computed tomography, Br. Poult. Sci. 55 (2014) 311–320.
[43] P. Arora, Z.M. Zhang, Battery separators, Chem. Rev. 104 (2004) 4419–4462.
[44] J.J. Zhang, Z.H. Liu, Q.S. Kong, C.J. Zhang, S.P. Pang, L.P. Yue, X.J. Wang, J.H. Yao, G.L. Cui, Renewable and superior thermal-resistant cellulose-based composite nonwoven as lithium-ion battery separator, ACS Appl. Mater. Interface 5 (2013) 128–134.
[45] M. Xiong, H.L. Tang, Y.D. Wang, Y. Lin, M.L. Sun, Z.F. Yin, M. Pan, Expanded polytetrafluoroethylene reinforced polyvinylidenefluoride–hexafluoropropylene separator with high thermal stability for lithium-ion Batteries, J. Power Sources 241 (2013) 203–211.
[46] N. Wu, Q. Cao, X.Y. Wang, Q.Q. Chen, Study of a novel porous gel polymer electrolyte based on TPU/PVdF by electrospinning technique, Solid State Ion. 203 (2011) 42–46.
[47] Y. Xie, H.L. Zou, H.F. Xiang, R. Xia, D.D. Liang, P.C. Shi, S. Dia, H.H. Wang, Enhancement on the wettability of lithium battery separator toward nonaqueous electrolytes, J. Membr. Sci. 503 (2016) 25–30.
[48] J.Y. Kim, D.Y. Lim, Surface-modified membrane as a separator for lithium–ion polymer battery, Energies 3 (2010) 866–885.
[49] K.S. Liu, X. Yao, L. Jiang, Recent developments in bio-inspired special wettability, Chem. Soc. Rev. 39 (2010) 3240–3255.
[50] S.S. Zhang, A review on electrolyte additives for lithium–ion batteries, J. Power Sources 162 (2006) 1379–1394.
[51] R. Prasanth, V. Aravindan, M. Srinivasan, Novel polymer electrolyte based on cob-web electrospun multicomponent polymer blend of polyacrylonitrile/poly(methyl methacrylate)/polystyrene for lithium ion batteries–preparation and electrochemical characterization, J. Power Sources 202 (2012) 299–307.
[52] L. Jabbour, M. Destro, C. Gerbaldi, D. Chaussy, N. Penazzi, D. Beneventi, Aqueous processing of cellulose based paper–anodes for flexible Li–ion batteries, J. Mater. Chem. 22 (2012) 3227–3233.
[53] D.C. Lin, Y.Y. Liu, Z. Liang, H.W. Lee, J. Sun, H.T. Wang, K. Yan, J. Xie, Y. Cui, Layered reduced graphene oxide with nanoscale interlayer gaps as a stable host for lithium metal anodes, Nat. Nanotechnol. 11 (2016) 626–632.
[54] H. Wang, C.L. Wang, E. Matios, W.Y. Li, Critical role of ultrathin graphene films with tunable thickness in enabling highly stable sodium metal anodes, Nano Lett. 17 (2017) 6808–6815.
[55] S.J. Chun, E.S. Choi, E.H. Lee, J.H. Kim, S.Y. Lee, S.Y. Lee, Eco–friendly cellulose nanofiber paper–derived separator membranes featuring tunable nanoporous network channels for lithium-ion batteries, J. Mater. Chem. 22 (2012) 16618–16626.
[56] W. Jiang, Z.H. Liu, Q.S. Kong, J.H. Yao, C.J. Zhang, P.X. Han, G.L. Cui, A high temperature operating nanofibrous polyimide separator in Li–ion battery, Solid State Ion. 232 (2013) 44–48.